An Interlaboratory Study on the Stability of All-Printable Hole Transport Material–Free Perovskite Solar Cells

De Rossi, Francesca; Barbé, Jérémy; Tanenbaum, David M.; Cinà, Lucio; Castriotta, Luigi Angelo; Stoichkov, Vasil; Wei, Zhengfei; Tsoi, Wing Chung; Kettle, Jeffrey; Sadula, Artem; Chircop, John; Azzopardi, Brian; Xie, Haibing; Di Carlo, Aldo; Lira-Cantú, Monica; Katz, Eugene A.; Watson, Trystan M.; Brunetti, Francesca

Energy technology

DOI:
10.1002/ente.202000134

Published: 01/12/2020

Peer reviewed version

An inter-laboratory study on the stability of all-printable HTM-free perovskite solar cells

Francesca De Rossi, Jérémy Barbé, David M. Tanenbaum, Lucio Cinà, Luigi A. Castriotta, Vasil Stoichkov, Zhengfei Wei, Wing Chung Tsoi, Jeffrey Kettle, Artem Sadula, John Chircop, Brian Azzopardi, Haibing Xie, Aldo Di Carlo, Monica Lira-Cantú, Eugene A. Katz, Trystan M. Watson, and Francesca Brunetti*

Dr. F. De Rossi, L.A. Castriotta, Prof. A. Di Carlo, Prof. F. Brunetti
CHOSE (Centre for Hybrid and Organic Solar Energy), Department of Electronic Engineering, University of Rome Tor Vergata, Via del Politecnico 1, Rome, 00133, Italy
E-mail: francesca.de.rossi@uniroma2.it

Dr. F. De Rossi, Dr. J. Barbé, Dr. V. Stoichkov, Dr. Z. Wei, Dr. W.C. Tsoi, Prof. T.M. Watson
Swansea University, Bay Campus, Fabian Way, Swansea, SA1 8EN, United Kingdom

Dr. D. Tanenbaum
Pomona College, Claremont, 91711, California, USA

Dr H. Xie, Prof. M. Lira-Cantú
Catalan Institute of Nanoscience and Nanotechnology (ICN2), CSIC and the Barcelona Institute of Science and Technology (BIST). Building ICN2, Campus UAB E-08193, Bellaterra, Barcelona, Spain

Dr. L. Cinà
Cicci Research s.r.l. Via Giordania 227 Grosseto 58100 Italy

Dr. J. Kettle
School of Computer Science and Electronic Engineering, Bangor University, Dean St, Bangor, Gwynedd, LL57 1UT, Wales, United Kingdom

Dr. A. Sadula, J. Chircop, Dr. Brian Azzopardi
MCAST Malta

Prof. Eugene A. Katz
Department of Solar Energy and Environmental Physics, Swiss Institute for Dryland Environmental and Energy Research, Jacob Blaustein Institutes for Desert Research, Ben-Gurion University of the Negev, Midreshet Ben-Gurion 8499000, Israel

Keywords: perovskite solar cells, carbon, long-term stability, ISOS protocols, inter-laboratory study

Abstract

Comparison between different laboratories on long-term stability analyses of perovskite solar cells (PSCs) is still lacking in the literature. This work presents the results of an inter-laboratory study carried out between 5 laboratories from 4 countries. Carbon-based PSCs were prepared by screen printing, encapsulated and sent to different laboratories across Europe to assess their stability by the application of three ISOS aging protocols: (a) in the dark (ISOS-D), (b) under simulated sunlight (ISOS-L) and (c) outdoors (ISOS-O). Over 1000 hours stability is reported for devices in the dark, both at room temperature and at 65 °C. Under continuous illumination at open circuit, cells survived only for few hours, although they recovered after being stored in the dark. Better stability is observed for cells biased at maximum power point under illumination. Finally, devices operate in outdoors for 30 days, with minor degradation, in two different locations (Barcelona, Spain and Paola, Malta). Our findings demonstrate that open circuit conditions are too severe for stability assessment and that the diurnal variation of the PV parameters reveals performance to be strongly limited by the fill factor, in the central hours of the day, due to the high series resistance of the carbon electrode.

1. Introduction

The efficiency of hybrid organic-inorganic metal halide perovskite solar cells (PSC)[1,2] has rapidly reached up to over 25% in the past few years.[3] Nonetheless, several factors have been demonstrated to induce PSC degradation, e.g. light,[4,5] temperature,[6,7] oxygen,[8,9] humidity,[10,11] electrical bias,[12–14] limiting the operational stability of such efficient devices and thus their commercialization.

In the wide range of possible device architectures and material combinations demonstrated so far for PSCs, carbon-based HTM-free PSCs (C-PSC) are one of the most promising, in terms of ease of manufacture,[15] environmental impact,[16] and long-term stability.[17]

Consisting of an all-printable triple mesoscopic stack, i.e. titania (TiO_2) electron transport layer, zirconia (ZnO_2) insulating layer and carbon-based back electrode, they show great potential as a low-cost PV technology for industrial production. Efforts have been concentrated to improve the manufacturing process[18–23] and large C-PSC modules have already been reported by different groups, with power conversion efficiency (PCE) ranging between 6 and 11%.[4,6–10]

When considering small cells ($\leq$ 1 cm^2 of active area), C-PSCs lag behind other PSC architectures that have recently exceeded 25% efficiency.[3] Regardless, a certified PCE as high as 12.84% has been reported for the MAPI infiltrated TiO_2/ZrO_2/C stack[15] while the record PCE ranges between 16% for a triple cation perovskite absorber, infiltrated in the same triple mesoscopic structure,[26] and 17% for a PIN structure, also endowed with a triple cation perovskite plus a nickel oxide layer between the insulator and the carbon electrode.[27]

An important milestone in their development was the addition of 5-AVAI (5-ammonium valeric acid iodide) to the perovskite precursors' solution: it has been proved to induce the formation of a peculiar multi-dimensional 2D/3D perovskite junction, i.e. AVA-MAPI, featuring both the enhanced stability of 2D perovskites and the broad absorption and excellent charge transport of 3D MAPI.[17,28] The additive located at grain boundaries also passivates surface defects, limiting the oxygen induced degradation.[29] Whilst lower in efficiency, C-PSC devices, endowed with AVA-MAPI perovskite, have demonstrated remarkable stability under illumination, both indoor at 1 sun, AM1.5 (> 1 year [17]) and outdoor (30 days, in Wuhan, China;[25] 2136 hours, i.e. 89 days, near Beijing, China[30]). In all these reports, assessment of the stability was conducted by the manufacturer, rather than through independent verification from an alternate laboratory, which is common practice in this field. Round robin stability studies on PSC are still limited, however as the technology matures, such studies will provide vital insight into testing protocols and variability in the stability from different testing approaches.[13,31–33]

This work assesses the stability of C-PSCs under a variety of conditions and involves measurements at 5 independent laboratories across Europe (UK, Italy, Spain, Malta) for measurements and characterisation, following the example set by the OPV community, who has promoted and widely participated in round robins and inter-laboratory studies.[34–37]

C-PSCs were manufactured by screen printing and infiltrated with AVA-MAPI solution at a single manufacturing site, encapsulated and then sent to different laboratories for characterisation in accordance with three ISOS protocols:[38] in the dark (ISOS-D), under simulated sunlight (ISOS-L), and outdoors (ISOS-O). Although this work was conducted in line with previous ISOS guidelines, which were established for OPV,[38] the work aligns with the new ISOS consensus stability standards for PSCs that has been published very recently.[39] Additional material characterisation measurements were performed to better understand the behaviour of the devices.

2. Results and discussion

C-PSCs used in this work consisted of a compact TiO_2 (c-TiO_2), deposited by spray pyrolysis on an FTO-glass covered, and three printed mesoporous layers: titania (m-TiO_2), zirconia (m-ZrO_2) and carbon (**Figure 1** a). While the former two layers have similar porosity and are hardly distinguishable, the over 10 μm thick carbon layer is made of both large graphite flakes and fine carbon black particles, as shown by the cross-section SEM (Figure 1 b). The energy dispersive X-ray spectroscopy (EDX) images (Figure 1 c) reveal that TiO_2 and ZrO_2 layers are about 0.8 μm and 1.2 μm respectively and, according to the uniform distribution of lead and iodine elements, the perovskite is infiltrated throughout the stack.

2.1. Photovoltaic performance of as-prepared devices

J-V measurements on 21 devices, masked to 0.5 cm^2 active area, returned a spread distribution of PCE values both prior to (around 4.6% in average - reverse scan) and after encapsulation

(around 5.4% in average - reverse scan), but no remarkable degradation, as shown in **Figure 2**a. A slight improvement in performance, primarily from changes in open circuit voltage (V_{OC}) and fill factor (FF), was noted after encapsulation along with a decrease in J_{SC} (**Figure S1**). As reported above, cells with the same structure ($TiO_2/ZrO_2/C$) and more conductive carbon electrode, infiltrated with the same perovskite, can deliver up to 12% PCE on a masked area of 0.07 cm^2 (printed area = 0.5 cm^2).[15] Herein, the choice of carrying out all measurements on 0.5 cm^2 masked active areas (printed area = 1 cm^2) explains the PCE values below 10%: reducing the masked active area from 0.5 cm^2 to 0.0625 cm^2 boosted the reverse scan PCE from 5.6% (5.2% forward scan, 5.4% stabilized at maximum power point – **Figure S2**) up to 9.3% (7.7% forward scan), as shown in Figure 2b. As well as for similar cells infiltrated with MAPI,[40] the dependence of the performance on the masked area is due to limitations in the conductivity of the carbon layer, affecting the series resistance, thus the fill factor (FF), as clearly shown by the slope of the J-V curve around V_{OC}. J_{SC} values also depended on the masked area, suggesting a non-homogenously infiltrated perovskite, possibly hindered by dense carbon flakes.[41] Despite the lower performance, 0.5 cm^2 masks were used throughout the study to allow sampling a more representative portion of the devices. IPCE spectra returned values of integrated J_{SC} consistent with those obtained by the J-V scans under the solar simulator (Figure S2). Encapsulated devices were shipped by air to the other partners for stability assessment and further characterization, as detailed in **Table 1**. Once the cells were received and before conducting stability tests, devices were measured at the characterization laboratory, by performing J-V scans in reverse and forward directions at the same scan rate as at the manufacturing laboratory, i.e. 20 mVs^{-1}. No remarkable degradation due to the shipping time or, in general, to the delay between fabrication by the manufacturing laboratory and testing by the characterization laboratories was observed, as shown in **Figure S3** for the cells used for the ISOS-O2 test in Barcelona (Spain).

2.2. Stability analysis in the Dark (ISOS-D)

In the dark, both at room temperature (ISOS D1) and at 65 °C (ISOS D2), the encapsulated devices proved to be remarkably stable. Interestingly, at room temperature (**Figure 3**, top), they suffered from an initial loss in performance, primarily due to a decrease of the V_{OC} (**Figure S4**), which led to a drop of around 20% in the initial PCE in 75 hours (T_{80}), although this stabilised afterwards without any further decrease for over 1000 hours. By contrast, when subjected to elevated temperature at 65 °C (Figure 3, bottom), the cells experienced a 20% improvement in the average performance within the first 3-4 hours; such improvement was then retained for almost 2000 hours, without seeing any further drop in performance. In this case though, the V_{OC} decreased in the first few hours, but this was offset by an increase in the J_{SC} (**Figure S5**), leading to the overall PCE improvement. AVA-MAPI perovskite for C-PSCs were (in this case) and usually are annealed at low temperature, i.e. 50 °C, thus prolonged exposure to 65 °C led most likely led to further annealing of the absorber layer with an improvement of the perovskite crystallinity and/or interfaces quality, i.e. better contact between perovskite and mesoscopic layers.

On the devices aged in the dark, Raman spectroscopy was applied to probe the degradation products within a perovskite device stack. One of the main by-products of perovskite degradation is lead iodide (PbI_2), which has a strong Raman signal, when excited with 532 nm laser[42], and such signal intensity is sensitive to the amount of PbI_2 formed in the perovskite, which can then be related to the film and/or device degradation. The PbI_2 peak can be detected as long as sufficient light reaches the PbI_2 formed at the interfaces and/or in the bulk of the perovskite film.

In a carbon-based PSC, the absorber layer is infiltrated all the way through the mesoporous layers. Hence, the perovskite and degradation products formed within the perovskite can be detected and monitored either from the glass/m-TiO_2 side or from the air/carbon side. The

penetration depth of 532 nm laser source into $CH_3NH_3PbI_3$ active layer is approximately 500 nm, which is much less than the total thickness of the carbon layer (i.e. >10 μm). Thus, the Raman signal from the carbon side will be indicative of perovskite and PbI_2 formed near the surface of the carbon layer only. On the other hand, measuring the device stack from the glass side will give information about perovskite and degradation products formed in the mesoporous TiO_2 layer only (~ 700 nm thick), i.e. in the photoactive part of the stack, where charge carriers are generated.

Raman measurements were thus performed on encapsulated cells, before and after ageing for 1200 h in the dark at room temperature and ambient humidity (ISOS-D1), and on non-encapsulated devices for comparison. The Raman spectra for the fresh encapsulated and non-encapsulated samples measured from the carbon side are shown in **Figure 4** (a and b). For the encapsulated sample, typical Raman spectrum of $CH_3NH_3PbI_3$ is observed with two broad and weak peaks at 110 cm^{-1} and 250 cm^{-1}, which were assigned to the vibrational and torsional modes of the methyl ammonium (MA) cations, respectively.[43] For the non-encapsulated sample, a completely different spectrum is measured, which shows sharp and intense peaks at 73 cm^{-1}, 96 cm^{-1} and 106 cm^{-1} indicatives of the presence of a large amount of PbI_2 [44] near the carbon surface, along with non-degraded perovskite, as revealed by the broad and poorly resolved peak centered at 242 cm^{-1}. Hence, the perovskite film near the surface of the device has already initiated degradation shortly after fabrication due to exposure to air when the device is not encapsulated, since some PbI_2 is formed alongside $CH_3NH_3PbI_3$.

After aging, different spectra are observed when measuring the devices from the carbon side (Figure 4c and Figure 4d, black lines). In the case of the encapsulated sample, no PbI_2 is measured near the surface but two small peaks at 110 cm^{-1} and 165 cm^{-1} were observed, which could be due to the formation of dihydrate perovskite $(CH_3NH_3)_4PbI_6 \cdot 2H_2O$, as shown in an earlier report.[42] The presence of dihydrate perovskite suggests that small amount of water

could have been trapped in the stack during the fabrication process and/or the encapsulation, both carried out in air. Still, the encapsulating glass seems to work as a barrier to environmental moisture and oxygen, preventing further degradation of the perovskite to PbI_2. For the non-encapsulated sample, intense PbI_2 signal is measured from the carbon side, and the perovskite Raman bands are not observed anymore (the additional peak at 215 cm^{-1} is an overtone of 109 cm^{-1} peak of PbI_2 as described by Warren et al. [44]). This clearly indicates the conversion of perovskite to PbI_2 in the carbon layer, near the surface, during the aging process.

By contrast, when the aged samples are measured from the mesoporous TiO_2 side (Figure 4c and Figure 4d, red lines), PbI_2 is not detected for either the encapsulated or the non-encapsulated samples. Instead, the band centered at 250-253 cm^{-1} indicates non-degraded perovskite and the peak at 144 cm^{-1} matches well with anatase TiO_2:[43,45] the perovskite infiltrated within the mesoporous TiO_2 layer was well preserved and did not undergo any major degradation, even without encapsulation. This correlates well with the performance of the devices, as summarized in **Table S1**: there is no degradation of the efficiency after 1200 h of ageing for both the encapsulated and non-encapsulated samples, and even a slight improvement in reverse bias. Indeed, Raman measurements showed that although the perovskite is degraded in the carbon electrode without encapsulation, it remains unchanged in the photoactive layer, where charges are generated (**Figure S6**), which explains the good stability in the dark of both the encapsulated and non-encapsulated carbon-based PSC.

2.3. Stability analisis under light irradiation at 1 sun (ISOS-L)

The high stability observed under ISOS-D1 and D2 conditions was not replicated under continuous illumination at open circuit at room temperature (in accordance with ISOS-L1 tests) nor at 65°C (ISOS-L2): in both instances, the performance dramatically dropped in few hours, regardless the temperature (**Figure 5**). Cells used for ISOS-L1 and L2 tests were retested one month after light soaking and they did still work, confirming that, also for this cell architecture,

storage in the dark for a sufficiently long time can induce performance recovery.[12,33] In this case, the recovery was only partial; still, around the 80% of the initial value was regained, due to a slight V_{OC} rise coupled to an irreversible J_{SC} drop of almost 50%, that, as a consequence, boosted the FF to higher values than at the beginning of the test, mitigating the loss in performance (**Figure S7** and **Figure S8**).

It is well known that an open circuit bias can accelerate the degradation during light soaking tests:[12] non extracted photogenerated charges accumulate and lead to high concentrations of radicals, which, in presence of oxygen and light, degrade the device.[9,29]

Also, the spectrum from a sulphur plasma lamp is broader than that of white LEDs, which do not include UV and IR radiation, limiting the optical excitation to the visible spectrum and thus degradation. Cells were then tested under white LEDs at maximum power point (MPP) by dynamically tracking it with a Perturb & Observe algorithm. The main PV parameters were recorded every 20 minutes with a JV scan. Degradation occurred also in this case, but, as expected, at a slower rate than at open circuit, with T_{80} reached after 79 hours (Figure 5c).

The inset shows the MPP dynamic behaviour after each JV scan: the JV hysteresis directly affects the time required to reach the steady-state MPP. As demonstrated by Pockett et al[46] for similar device structure, the slow response time under illumination can be related to the formation of 2D perovskite regions which restrict ion migration, a phenomenon that is promoted by the AVA additive.

The evolution of V_{OC} and J_{SC} with light intensity (P_{inc}) can provide information about the recombination phenomena within the device. **Figure 6** shows semi-logarithmic plots of the V_{OC} versus light intensity for the C-PSC before and after light-soaking at MPP. At low light levels (< 0.01 Wcm^{-2}), the aged devices show an increased slope of the V_{OC} (from 165 to 251 mV/dec), in particular, as demonstrated by Gouda et al,[47] at these irradiation levels the increase of V_{OC} is limited by the TiO_2 and the accumulation of the photo-injected electrons, similar to dye

sensitized solar cells. This is a clear indication of a severe photoinduced degradation of the mesoporous layer.

Additional information about recombination processes can be extrapolated by the power law fit of the J_{SC} trend at different light intensities, before and after the stability test. The reduction of the power index (γ) from 0.91 to 0.88 is an evident indication of the appearance of bimolecular recombination processes induced by the light stress that degrades the charge collection capability[48].

2.4. Stability analysis outdoors (ISOS-O)

Outdoor measurements were carried out in two different sites, i.e. Barcelona, Spain (41° 30' 5.56" N, 2° 6' 39.68" W) and Paola, Malta (35° 52' 53.04" N, 14° 30' 42.26" E), accordingly to the ISOS-O2 protocol, i.e. by performing J-V scans *in-situ* under natural illumination. It is worth noting that while in Barcelona the testing system available was a 2-axys tracking one, in Malta it was fixed, both allowed by the ISOS protocols. For standard operating procedures, internal and specific to each laboratory, UV filters were used in Barcelona but not in Malta. Nevertheless, in both locations, as shown in **Figure 7**, cells were stable for several weeks (between 700 and 800 hours, i.e. around 30 days). Cells were still working when data collection ended, and IPCE spectra were remeasured indoors: little variation is observed compared to the spectrum at the beginning of the test (**Figure S9**). These stability measurements add further evidence of the good outdoor performance of this PSC architecture to previously published reports by other groups of one-week stability in Jeddah, Saudi Arabia,[49] 30 days in Wuhan, China[25] and nearly 90 days in location near Beijing, China, with temperatures ranging between -10 and 35 °C.[30]

As the tests were carried out between April and June (late spring – summer at the given latitudes) in Southern Europe, temperatures were above 20 °C during the central hours of the day and above 6 °C at night, whereas irradiation levels peaked near 1000 Wm^{-2} were achieved

around midday in sunny days. Irradiance levels dropped during cloudy days and so did the photogenerated current, but overall, the performance was not affected, as the detrimental effect on J_{SC} was offset by the FF improvement.

Although Figure 7 shows only midday values of the recorded temperature, irradiance and PV parameters, in one site (Barcelona), C-PSC outdoor operation was also tracked from early morning to late evening, making possible single-day analysis of the device response under variable irradiation levels and temperatures. J-V curves were performed every 45 minutes, at a scan rate of 20 mVs^{-1} in both forward and reverse direction. The evolution of all the parameters over 3 days, from around 8:00 am to around 8:00 pm, is shown in **Figure 8**. Temperatures were lower in the morning, high and quite constant in the central hours and still around 20 °C even in the late evening. The J_{SC} trend mimicked the evolution of the irradiation and V_{OC} was fairly constant over the hours, with a slight drop at about 8 am and 8 pm. Large FF values were observed in the early morning and late evening while they significantly dropped in the central hours when the temperature and irradiation were around their maximum: the high series resistance of the carbon electrode affected the FF as the irradiation levels and the photogenerated currents increased, limiting the PCE in the central hours of the day. Temperature as well as variable spectral composition of sunlight during the day could explain the asymmetrical PCE trend, with the highest values in the late evening. It is worth noting that a similar behaviour (higher PCE values at the beginning and end of the day) has been reported also for NiOx/MAPI/PCBM[50] and m-TiO_2/mixed cation-halide perovskite/spiro[31] devices.

As for other PSC architectures, the response of these C-PSC devices in terms of stability depend on the applied ageing conditions and can be explained by the different types of degradation, i.e. reversible or permanent, that are triggered in each case. As previously reported for mixed cation-halide perovskites on both m-TiO_2 and SnO_2 based cells,[31,33,51] this work demonstrates that printable C-PSC cells can degrade beyond the threshold of reversible losses under

continuous illumination (faster at open circuit than when tracking the maximum power point) and have their efficiency dropping quickly, even if a partial recovery is possible upon a long enough time of storage in the dark; whereas, over light/dark cycles such as in an outdoor test, the degradation can be reversible and cells recover overnight, leading to a remarkable ~30 days stable operation in two different sites.

3. Conclusion

We have carried out an inter-laboratory stability analyses of C-PSCs fabricated under controlled conditions by different laboratories. Analyses were performed following several ISOS protocols (ISOS-D1, D2, L1, L2, O2), applied by different laboratories to assess the stability of printed, HTM-free Carbon-based PSC cells based on a triple mesoscopic stack with a carbon back electrode. Whilst showing over 1000 h stability in the dark at both room temperature and 65 °C, these devices suffered notable performance drop when tested under continuous illumination in open circuit conditions. Maximum power point tracking and LED illumination resulted in slower degradation, as already demonstrated for other PSC architecture. Finally, cells diurnal outdoor operation was tracked for several days, showing higher PCE values in the early morning and late evening and a drop in the central hours of the day, due to the high series resistance of the carbon electrode that limits the fill factor. Nonetheless, devices were stable for about 30 days of outdoor operation in two different sites, confirming that, for this architecture, the natural day/night cycling, i.e. real-world conditions, is beneficial to the long-term operation and it is a more realistic approach to assessing the stability and lifetime for C-PSC devices. Since light/dark cycles can be reproduced also indoors, they should be included in long-term stability studies, as agreed on in the new ISOS protocols.[39]

4. Experimental Section

Cells fabrication: FTO glass substrates (TEC7, XOP) were etched using a Rofin Nd:YVO_4 laser (532 nm) at a speed of 150 mm s^{-1}, cleaned with Hellmanex solution in deionised water, washed with deionised water and rinsed in acetone and isopropanol, before being O_2 plasma treated. A 50 nm-thick compact TiO_2 layer was deposited via spray pyrolysis at 300°C from a solution 1:9 of titanium di-isopropoxide bis(acetylacetonate) (Sigma) in isopropanol. The triple mesoporous stack was obtained via screen printing of commercial pastes: first, the TiO_2 layer (30 NRD Dyesol, diluted 1:1 by weight with terpineol), followed by sintering at 550°C for 30 minutes; then the ZrO_2 layer (Solaronix), sintered at 400°C for 30 minutes; finally, the carbon layer (Gwent Electronic Materials), sintered at 400°C for 30 minutes. A solution of AVAI, MAI and PbI_2 in gamma-butyrolactone (GBL) was prepared according to Jiang et al[52] infiltrated from the top carbon electrode, percolated throughout the mesoporous stack down to the TiO_2, filling the pores and, within them, slowly crystallizing into perovskite during the annealing at 50 °C for 1 hour.

Silver paint was applied to the contacts and a black tape mask to the glass side, with an aperture of 0.5 cm^2 to univocally define the active area, allowing consistency for samples measured in different laboratories. All cells were encapsulated in air using a plain glass cover and a UV-curable epoxy for edge sealing (primary encapsulation). Curing was performed under a UV lamp for few seconds, having care of exposing only the epoxy around the glass cover edges. Cells meant for outdoor testing had wires ultrasonically soldered to the contacts to make possible the addition of a UV filter and a secondary encapsulation of waterproof silicone (**Figure S10**).

Indoor ISOS tests: Prior to shipping, the cells were characterised at the manufacturer laboratory. JV measurements were performed using in-house developed software and a Keithley 2400 source meter under a class AAA solar simulator (Newport Oriel Sol3A equipped with a sulphur plasma lamp) at AM1.5 illumination conditions calibrated at 1 sun against a KG5 filtered silicon reference cell (Newport Oriel 91150-KG5). The cells were scanned in reverse (from V_{OC} to J_{SC})

and forward directions at a scan rate of 20 mV/s. For the stabilised measurements, a bias, set to the voltage at maximum power point as determined by the JV sweep, was applied and the current monitored under illumination. The active area of solar cells was defined through a laser-cut mask with an open area of 0.5 cm^2. Incident photons to current efficiency (IPCE) spectra were collected using a QE X10 spectral response machine in the 300-850 nm wavelength range. Once received by the characterization laboratory and before starting the stability tests, they were measured again, using the same settings as in the manufacturing laboratory: 20 mV/s, for both reverse and forward scans between 1 V and -0.1 V.

Dark and thermal stress tests (ISOS-D1, ISOS-D2) were conducted using a Weiss Technik UK thermal-humidity chamber. Light soaking tests (ISOS-L1, ISOS-L2) were conducted using a sulphur plasma lamp (Class AAA) from Plasma-I in Germany with temperature-controlled stage. Irradiance levels were calibrated using a thermopile every 5 days. Current-Voltage and MPPT were conducted using a Keithley 2601.

Maximum power point tracking (MPPT) was performed using the commercial apparatus ARKEO (Cicci Research). The main PV parameters were recorded every 20 minutes with an I-V scan. The Maximum Power Point was dynamically tracked with a Perturb & Observe algorithm.

Outdoor ISOS tests in Barcelona (Spain): Upon receipt of cells, JV curves were measured indoors under a metal halide solar simulator lamp (AM 1.5G) and IPCE measurements were taken from 300 to 800 nm, both before and after the addition of a UV filter. Outdoor stability measurements were conducted on the encapsulated cells with UV filters and masks, using a 2-axis tracking system, and recording forward and reverse J-V curves (sweep rate 20 mVs^{-1}), temperature, and irradiance every ~45 min, when solar irradiance exceeded 50 Wm^{-2} as measured by the pyranometer on the solar tracker. Between measurements and when irradiance was below 50 Wm^{-2} cells were held at open circuit. Cells were re-measured in the lab after 30 days of outdoor measurements.

Outdoor ISOS tests in Paola (Malta):

Outdoor stability measurements were conducted on the encapsulated cells without UV filters and masks, using a fixed system with orientation 35° South, and recording forward and reverse J-V curves (sweep rate 20 mVs^{-1}), temperature, and irradiance every ~30 min, when solar irradiance is approximately 800 Wm^{-2} as measured by the pyranometer on the surface. Between measurements and when irradiance was below 800 Wm^{-2} cells were held at open circuit.

Further characterization:

Morphology and thickness of the mesoporous stack was studied using a JEOL-JSM-7800F field emission scanning electron microscope (5 kV acceleration voltage, a working distance of 10 mm and a magnification of 25,000x). Energy dispersive X-ray spectroscopy mapping was used to determine the element distribution using 20 kV acceleration voltage.

Raman measurements were performed with a Renishaw Invia Raman system in backscattering configuration. A 532 nm laser and 50x objective were used (Numerical Aperture: 0.50, spot size ≈ 1 μm). A laser power of 0.3 mW and acquisition time of 5 s were used. For each sample, 100 different spots were measured over the surface and averaged to increase the signal-to-noise ratio without degrading the cell by long laser exposure. The samples were analysed from both the carbon side and glass side to probe the perovskite degradation in the carbon or mesoporous TiO_2 film, respectively.

Light intensity dependent tests were performed using the commercial apparatus ARKEO (Cicci Research) endowed with a LED based illuminator (spectral emission from 450 nm to 750 nm) with 2 cm diameter of optical aperture. Devices were attached over a metal substrate to increase the thermal capacitance. No thermal control was applied to the device because the temperature variation was confined between 24 and 34 °C.

Supporting Information

Supporting Information is available from the Wiley Online Library or from the author.

Acknowledgements

This work was supported by the European Commission's StableNextSol COST Action MP1307.

F.D.R., Z.W., J.B., W.C.T. and T.W. would like to acknowledge the support provided from the Engineering and Physical Sciences Research Council (EPSRC) through the Self-assembling Perovskite Absorbers - Cells Engineered into Modules project (EP/M015254/1), the PhotoVoltaic Technology based on Earth-Abundant Materials project (EP/L017792/1), the High resolution mapping of performance and degradation mechanisms in printable photovoltaic devices project (EP/M025020/1) and the SPECIFIC Innovation and Knowledge Centre (EP/N020863/1); they would also like to express their gratitude to the Welsh Government for their support of the Sêr Solar programme.

J.K. and V.S. acknowledge the work and the support of the Solar Photovoltaic Academic Research Consortium II (SPARC II) project, gratefully funded by WEFO.

D.M.T. acknowledges sabbatical support from Pomona College and the opportunity to visit at both SPECIFIC and ICN2 to participate in this research.

D.M.T., M.L.C. and H.X. acknowledge the support from Spanish MINECO for the grant GraPErOs (ENE2016-79282-C5-2-R), the OrgEnergy Excellence Network CTQ2016-81911-REDT, the Agència de Gestió d'Ajuts Universitaris i de Recerca (AGAUR) for the support to the consolidated Catalonia research group 2017 SGR 329. ICN2 is supported by the Severo Ochoa program from Spanish MINECO (Grant no. SEV-2017-0706) and is funded by the CERCA Programme/Generalitat de Catalunya.

A.S. and B.A. would like to acknowledge the support from the European Commission H2020 TWINNING JUMP2Excel (Joint Universal activities for Mediterranean PV integration Excellence) project under grant 810809.

E.A.K. acknowledges the visiting professor fellowship from University of Rome Tor Vergata.

L.C. acknowledges ARIADNE project funded by the Tuscany region with POR-FESR 2014-2020.

F.B. and F.D.R. would like to acknowledge the European Union's Horizon 2020 research and innovation programme under grant agreement No763989 APOLO. This publication reflects only the author's views and the European Union is not liable for any use that may be made of the information contained therein.

Received: ((will be filled in by the editorial staff))
Revised: ((will be filled in by the editorial staff))
Published online: ((will be filled in by the editorial staff))

References

[1] S. He, L. Qiu, L. K. Ono, Y. Qi, *Mater. Sci. Eng. R Reports* **2020**, *140*, DOI 10.1016/j.mser.2020.100545.

[2] A. K. Jena, A. Kulkarni, T. Miyasaka, *Chem. Rev.* **2019**, *119*, 3036–3103.

[3] NREL, "Best Research-Cell Efficiency Chart | Photovoltaic Research | NREL," **2019**.

[4] F. Lang, O. Shargaieva, V. V. Brus, H. C. Neitzert, J. Rappich, N. H. Nickel, *Adv. Mater.* **2018**, *30*, 1702905.

[5] S. W. Lee, S. Kim, S. Bae, K. Cho, T. Chung, L. E. Mundt, S. Lee, S. Park, H. Park, M. C. Schubert, et al., *Sci. Rep.* **2016**, *6*, DOI 10.1038/srep38150.

[6] P. Holzhey, P. Yadav, S. H. Turren-Cruz, A. Ummadisingu, M. Grätzel, A. Hagfeldt, M. Saliba, *Mater. Today* **2019**, *29*, 10–19.

[7] G. Divitini, S. Cacovich, F. Matteocci, L. Cinà, A. Di Carlo, C. Ducati, *Nat. Energy* **2016**, *1*, 15012.

[8] N. Aristidou, C. Eames, I. Sanchez-Molina, X. Bu, J. Kosco, M. S. Islam, S. A. Haque, *Nat. Commun.* **2017**, *8*, 1–10.

[9] D. Bryant, N. Aristidou, S. Pont, I. Sanchez-Molina, T. Chotchunangatchaval, S. Wheeler, J. R. Durrant, S. A. Haque, *Energy Environ. Sci.* **2016**, *9*, 1655–1660.

[10] D. Li, S. A. Bretschneider, V. W. Bergmann, I. M. Hermes, J. Mars, A. Klasen, H. Lu, W. Tremel, M. Mezger, H. J. Butt, et al., *J. Phys. Chem. C* **2016**, *120*, 6363–6368.

[11] J. Yang, B. D. Siempelkamp, D. Liu, T. L. Kelly, *ACS Nano* **2015**, *9*, 1955–1963.

[12] K. Domanski, E. A. Alharbi, A. Hagfeldt, M. Grätzel, W. Tress, *Nat. Energy* **2018**, *3*, 61–67.

[13] A. K. M., M. V Khenkin, F. Di Giacomo, Y. Galagan, S. Rahmany, L. Etgar, E. A. Katz, I. Visoly-Fisher, *Sol. RRL* **2019**, 1900335.

[14] M. V. Khenkin, K. M. Anoop, E. A. Katz, I. Visoly-Fisher, *Energy Environ. Sci.* **2019**, *12*, 550–558.

[15] A. Mei, X. Li, L. Liu, Z. Ku, T. Liu, Y. Rong, M. Xu, M. Hu, J. Chen, Y. Yang, et al., *Science (80-.).* **2014**, *345*, 295–298.

[16] J. A. Alberola-Borràs, J. A. Baker, F. De Rossi, R. Vidal, D. Beynon, K. E. A. Hooper, T. M. Watson, I. Mora-Seró, *iScience* **2018**, *9*, 542–551.

[17] G. Grancini, C. Roldán-Carmona, I. Zimmermann, E. Mosconi, X. Lee, D. Martineau,

S. Narbey, F. Oswald, F. De Angelis, M. Graetzel, et al., *Nat. Commun.* **2017**, *8*, 1–8.

[18] A. Priyadarshi, L. J. Haur, P. Murray, D. Fu, S. A. Kulkarni, G. Xing, T. C. Sum, N. Mathews, S. G. Mhaisalkar, J. H. Lew, et al., *Energy Environ. Sci.* **2016**, *9*, 3687–3692.

[19] Y. Hu, S. Si, A. Mei, Y. Rong, H. Liu, X. Li, H. Han, *Sol. RRL* **2017**, *1*, 1600019.

[20] J. Baker, K. Hooper, S. Meroni, A. Pockett, J. McGettrick, Z. Wei, R. Escalante, G. Oskam, M. Carnie, T. Watson, *J. Mater. Chem. A* **2017**, *5*, 18643–18650.

[21] S. M. P. Meroni, Y. Mouhamad, F. De Rossi, A. Pockett, J. Baker, R. Escalante, J. Searle, M. J. Carnie, E. Jewell, G. Oskam, et al., *Sci. Technol. Adv. Mater.* **2018**, *19*, 1–9.

[22] S. M. P. Meroni, K. E. A. Hooper, F. De Rossi, P. Greenwood, J. Troughton, J. A. Baker, W. Dixon, D. A. Worsley, T. M. Watson, *Sol. Energy Mater. Sol. Cells* **2018**, (under review).

[23] F. De Rossi, J. A. Baker, D. Beynon, K. E. A. Hooper, S. M. P. Meroni, D. Williams, Z. Wei, A. Yasin, C. Charbonneau, E. H. Jewell, et al., *Adv. Mater. Technol.* **2018**, 1800156.

[24] A. Bashir, S. S. Shukla, J. H. Lew, S. S. Shukla, A. Bruno, D. Gupta, T. Baikie, R. Patidar, Z. Akhter, A. Priyadarshi, et al., *Nanoscale* **2018**, *10*, 2341–2350.

[25] Y. Hu, S. Si, A. Mei, Y. Rong, H. Liu, X. Li, H. Han, *Sol. RRL* **2017**, *1*, 1600019.

[26] Q. Wang, W. Zhang, Z. Zhang, S. Liu, J. Wu, Y. Guan, A. Mei, Y. Rong, Y. Hu, H. Han, *Adv. Energy Mater.* **2019**, 1903092.

[27] S. Liu, W. Huang, P. Liao, N. Pootrakulchote, H. Li, J. Lu, J. Li, F. Huang, X. Shai, X. Zhao, et al., *J. Mater. Chem. A* **2017**, *5*, 22952–22958.

[28] M. Lira-Cantú, *Nat. Energy* **2017**, *2*, DOI 10.1038/nenergy.2017.115.

[29] C. T. Lin, F. De Rossi, J. Kim, J. Baker, J. Ngiam, B. Xu, S. Pont, N. Aristidou, S. A. Haque, T. Watson, et al., *J. Mater. Chem. A* **2019**, *7*, 3006–3011.

[30] Z. Fu, M. Xu, Y. Sheng, Z. Yan, J. Meng, C. Tong, D. Li, Z. Wan, Y. Ming, A. Mei, et

al., *Adv. Funct. Mater.* **2019**, *29*, 1809129.

[31] Y. Reyna, M. Salado, S. Kazim, A. Pérez-Tomas, S. Ahmad, M. Lira-Cantu, *Nano Energy* **2016**, *30*, 570–579.

[32] M. V. Khenkin, K. M. Anoop, I. Visoly-Fisher, Y. Galagan, F. Di Giacomo, B. R. Patil, G. Sherafatipour, V. Turkovic, H. G. Rubahn, M. Madsen, et al., *Energy Environ. Sci.* **2018**, *11*, 739–743.

[33] M. V. Khenkin, K. M. Anoop, I. Visoly-Fisher, S. Kolusheva, Y. Galagan, F. Di Giacomo, O. Vukovic, B. R. Patil, G. Sherafatipour, V. Turkovic, et al., *ACS Appl. Energy Mater.* **2018**, *1*, 799–806.

[34] Y. Xiao, J. Wu, G. Yue, J. Lin, M. Huang, L. Fan, Z. Lan, *Electrochim. Acta* **2011**, *58*, 621–627.

[35] S. A. Gevorgyan, M. Corazza, M. V Madsen, G. Bardizza, A. Pozza, H. Müllejans, J. C. Blakesley, G. F. A. Dibb, F. A. Castro, J. F. Trigo, et al., *Polym. Degrad. Stab.* **2014**, *109*, 162–170.

[36] M. V Madsen, S. A. Gevorgyan, R. Pacios, J. Ajuria, I. Etxebarria, J. Kettle, N. D. Bristow, M. Neophytou, S. A. Choulis, L. Stolz Roman, et al., *Sol. Energy Mater. Sol. Cells* **2014**, *130*, 281–290.

[37] T. T. Larsen-Olsen, S. A. Gevorgyan, R. R. Søndergaard, M. Hösel, Z. Gu, H. Chen, Y. Liu, P. Cheng, Y. Jing, H. Li, et al., *Sol. Energy Mater. Sol. Cells* **2013**, *117*, 382–389.

[38] M. O. Reese, S. A. Gevorgyan, M. Jørgensen, E. Bundgaard, S. R. Kurtz, D. S. Ginley, D. C. Olson, M. T. Lloyd, P. Morvillo, E. A. Katz, et al., *Sol. Energy Mater. Sol. Cells* **2011**, *95*, 1253–1267.

[39] M. V. Khenkin, E. A. Katz, A. Abate, G. Bardizza, J. J. Berry, C. Brabec, F. Brunetti, V. Bulović, Q. Burlingame, A. Di Carlo, et al., *Nat. Energy* **2020**, *5*, 35–49.

[40] J. Baker, K. Hooper, S. Meroni, A. Pockett, J. McGettrick, Z. Wei, R. Escalante, G. Oskam, M. Carnie, T. Watson, *J. Mater. Chem. A* **2017**, *5*, 18643–18650.

[41] H. Lakhiani, T. Dunlop, F. De Rossi, S. Dimitrov, R. Kerremans, C. Charbonneau, T. Watson, J. Barbé, W. C. Tsoi, *Adv. Funct. Mater.* **2019**, *29*, 1900885.

[42] K. E. A. Hooper, H. K. H. Lee, M. J. Newman, S. Meroni, J. Baker, T. M. Watson, W. C. Tsoi, *Phys. Chem. Chem. Phys.* **2017**, *19*, 5246–5253.

[43] C. Quarti, G. Grancini, E. Mosconi, P. Bruno, J. M. Ball, M. M. Lee, H. J. Snaith, A. Petrozza, F. De Angelis, *J. Phys. Chem. Lett.* **2014**, *5*, 279–284.

[44] R. F. Warren, W. Y. Liang, *J. Phys. Condens. Matter* **1993**, *5*, 6407.

[45] A. Wypych, I. Bobowska, M. Tracz, A. Opasinska, S. Kadlubowski, A. Krzywania-Kaliszewska, J. Grobelny, P. Wojciechowski, *J. Nanomater.* **2014**, *2014*, DOI 10.1155/2014/124814.

[46] A. Pockett, D. Raptis, S. M. P. Meroni, J. Baker, T. Watson, M. Carnie, *J. Phys. Chem. C* **2019**, *123*, 11414–11421.

[47] L. Gouda, R. Gottesman, A. Ginsburg, D. A. Keller, E. Haltzi, J. Hu, S. Tirosh, A. Y. Anderson, A. Zaban, P. P. Boix, *J. Phys. Chem. Lett.* **2015**, *6*, 4640–4645.

[48] S. Shao, Z. Chen, H. H. Fang, G. H. Ten Brink, D. Bartesaghi, S. Adjokatse, L. J. A. Koster, B. J. Kooi, A. Facchetti, M. A. Loi, *J. Mater. Chem. A* **2016**, *4*, 2419–2426.

[49] X. Li, M. Tschumi, H. Han, S. S. Babkair, R. A. Alzubaydi, A. A. Ansari, S. S. Habib, M. K. Nazeeruddin, S. M. Zakeeruddin, M. Grätzel, *Energy Technol.* **2015**, *3*, 551–555.

[50] V. Stoichkov, N. Bristow, J. Troughton, F. De Rossi, T. M. Watson, J. Kettle, *Sol. Energy* **2018**, *170*, 549–556.

[51] K. Domanski, B. Roose, T. Matsui, M. Saliba, S. H. Turren-Cruz, J. P. Correa-Baena, C. R. Carmona, G. Richardson, J. M. Foster, F. De Angelis, et al., *Energy Environ. Sci.* **2017**, *10*, 604–613.

[52] X. Jiang, Y. Xiong, A. Mei, Y. Rong, Y. Hu, L. Hong, Y. Jin, Q. Liu, H. Han, *J. Phys. Chem. Lett.* **2016**, *7*, 4142–4146.

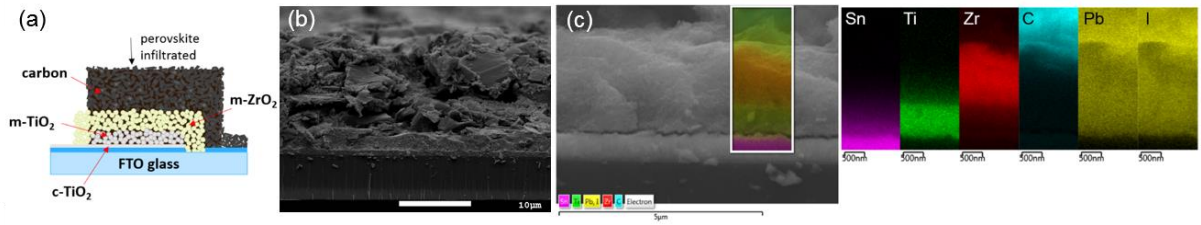

Figure 1. C-PSC used in this work. (a) Schematic representation of a typical cell; (b) Cross-section SEM image, showing the different layers of the device; (c) EDX elemental maps: Sn (FTO conductive layer), Ti (TiO_2 layer), Zr (insulating ZrO_2 layer), C (graphite/carbon black electrode), Pb and I (infiltrated perovskite throughout the stack).

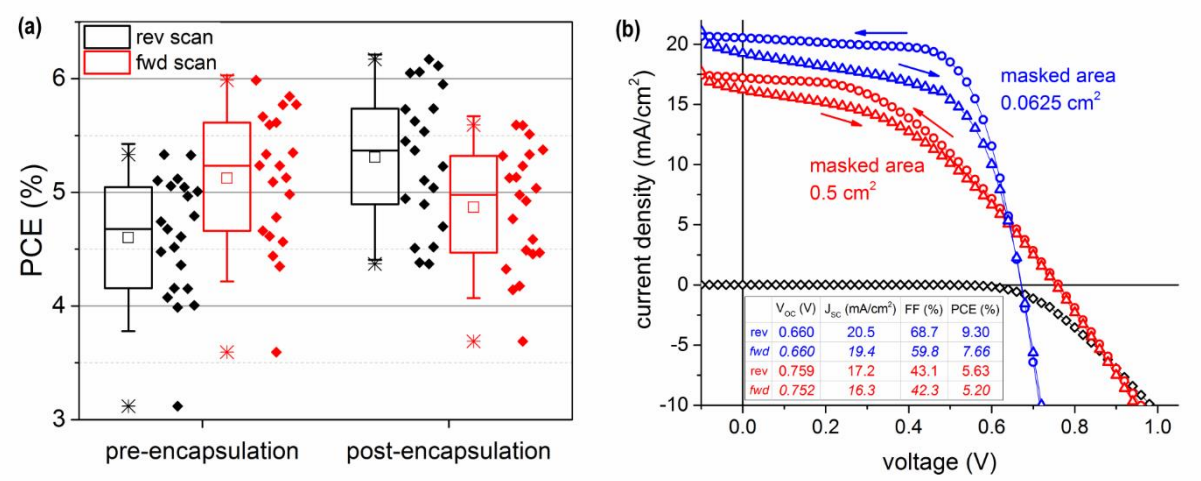

Figure 2. (a) PCE distribution of 21 cells, masked to 0.5 cm^2 area, before and after encapsulation; (b) typical JV curves for an encapsulated device with different masked areas. Scans were performed from 1 V to -0.1 V at 20 mVs^{-1}, in both reverse (V_{OC} to J_{SC}) and forward directions.

Table 1. Number of cells shipped to the different partners and tests performed, according to the ISOS definition.

No. of cells	Tests	Laboratory
12	ISOS D1, D2, L1, L2	Bangor University (UK)
2	ISOS O2	ICN2 Barcelona (Spain)
2	ISOS O2	MCAST Paola (Malta)
2	Raman spectroscopy	Swansea University (UK)
2	ISOS L1 (MPPT) and steady state measurements	University of Rome Tor Vergata (Italy)

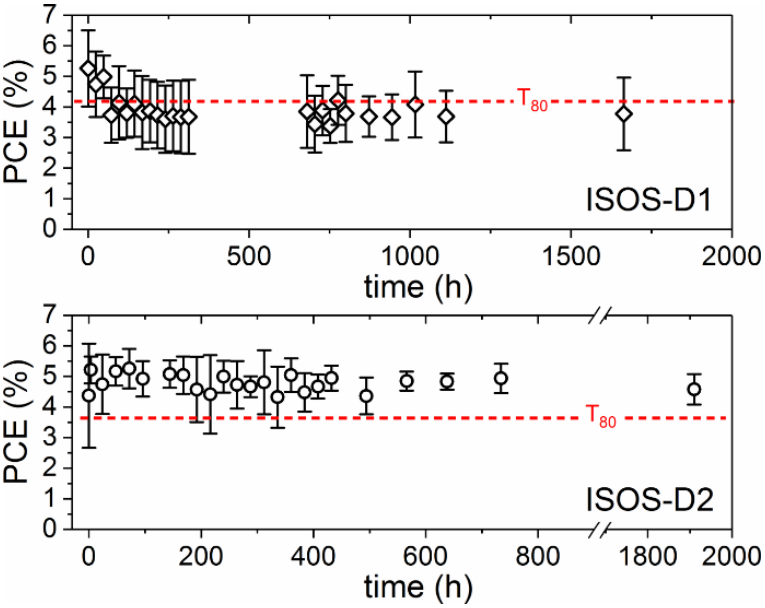

Figure 3. Stability analysis on C-PSC devices following ISOS-D1 (dark, room temperature, ambient humidity) and ISOS-D2 (dark, 65 °C, ambient humidity). Average of 3 cells, 0.5 cm^2 masked area. The dashed line indicates T_{80} value, i.e. the time when the PCE drops to 80% of its initial value. The remaining PV parameters are reported in Figure S3 and Figure S4.

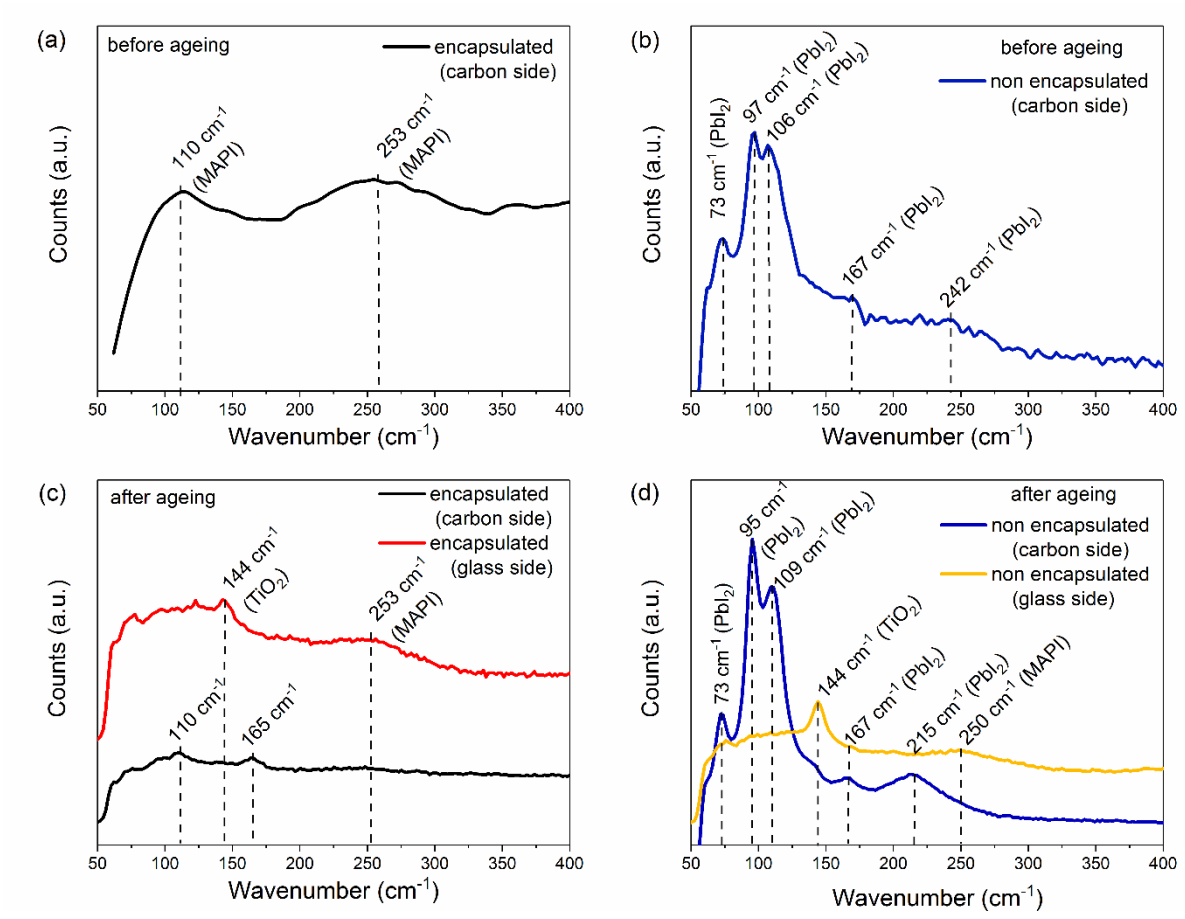

Figure 4. Raman spectra of C-PSC devices analysed under ISOS-D1 conditions (dark, room temperature, ambient humidity). (a, b) Freshly prepared, before ageing: encapsulated (a) and not encapsulated (b); after 1200 h of ageing: encapsulated (c) and not encapsulated (d). Carbon side and glass side refer to the direction the laser hit on the sample, respectively from the back through the carbon electrode and from the front through the conductive glass.

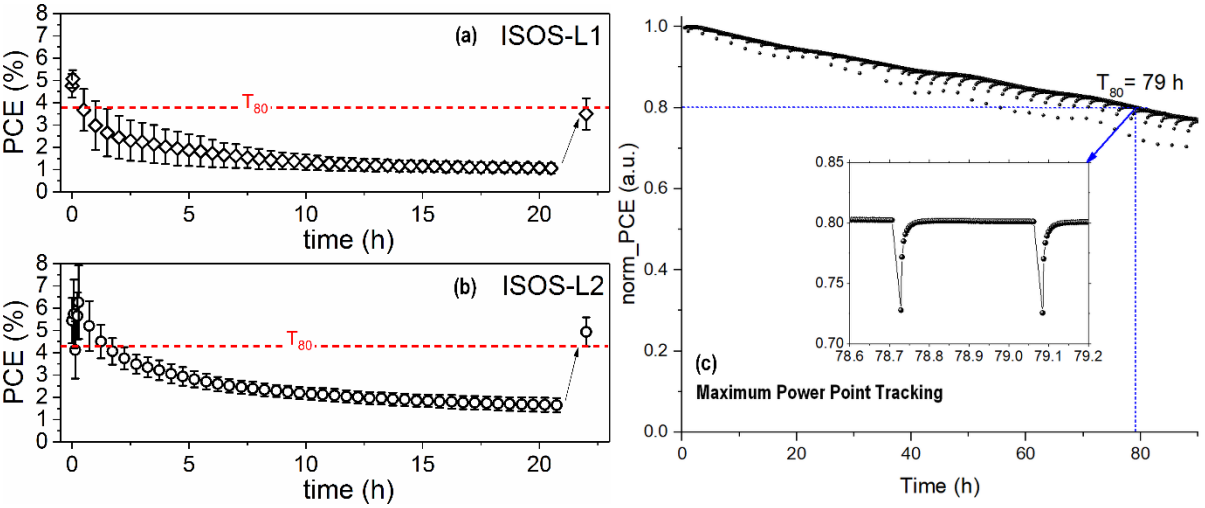

Figure 5. Stability tests on encapsulated C-PSCs, following ISOS-L protocols: (a-b) 1 sun from sulphur plasma lamp at open circuit, and (c) 1 equivalent sun from white LEDs, MMP tracking. (a) ISOS-L1 (room temperature, ambient humidity) and (b) ISOS-L2 (65 °C, ambient humidity). Reported data are averaged values over 3 devices with 0.5 cm^2 masked area. The cells were tested again once shipped back to the manufacturing laboratory, showing partial recovery. (c) ISOS-L1 (room temperature, ambient humidity) under LEDs at 1 equivalent sun, MPP tracking.

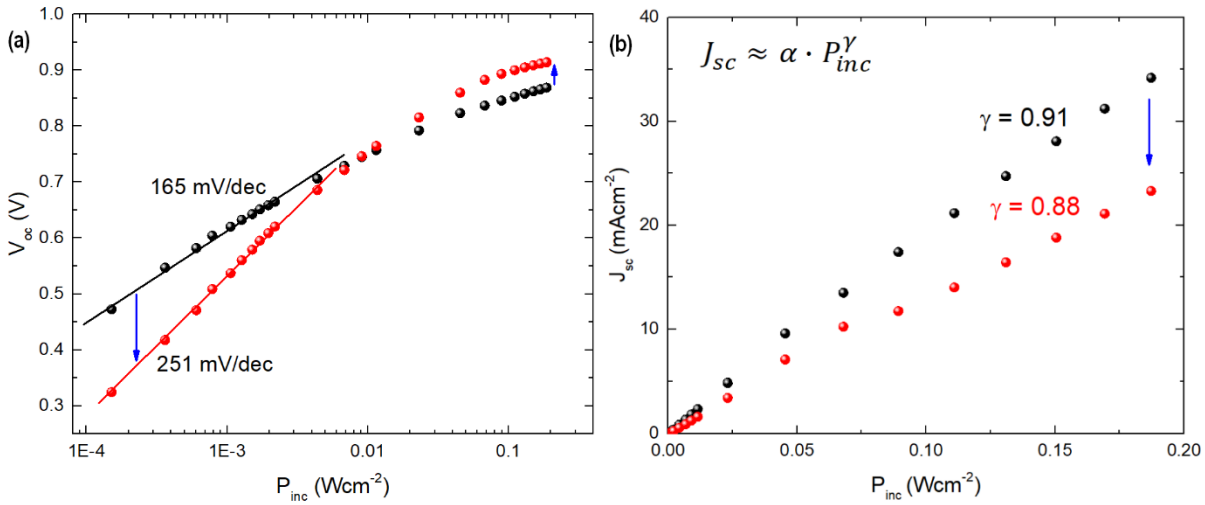

Figure 6. Comparison of C-PSC behaviour before (black symbols) and after (red symbols) the light soaking under white LED at MPP (ISOS-L1): (a) V_{OC} and (b) J_{SC} at different light intensities.

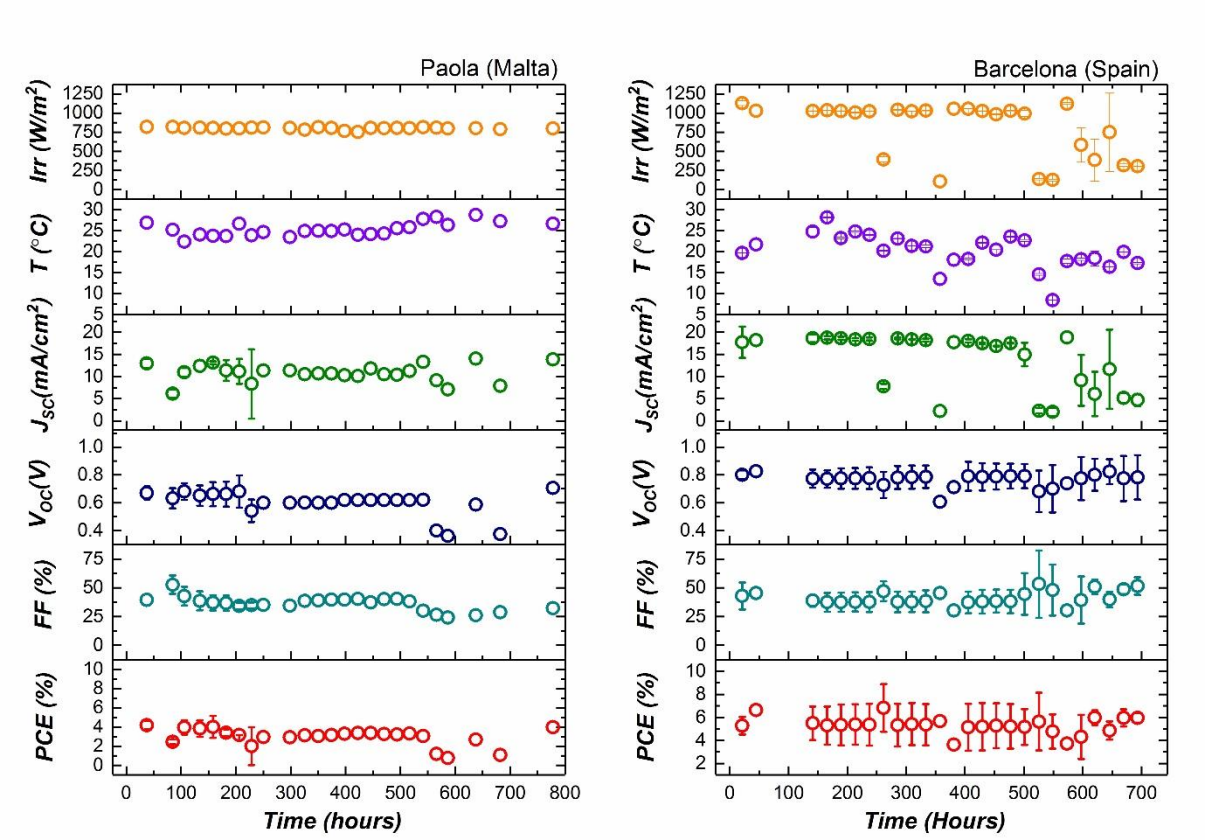

Figure 7. Stability analysis carried out on encapsulated C-PSCs according to protocol ISOS-O2 (outdoor tests): irradiance, temperature and PV parameters over time for cells tested in Paola, Malta (left, May-June) and Barcelona, Spain (right, April-May). In each location, 2 devices were tested (in Paola, one cell stopped working after 250 hours). Plotted data refer to midday measurements. UV filters and a 2-axys tracking system were used for the cells tested in Barcelona. A fixed system and no UV filters were used for the cells tested in Malta.

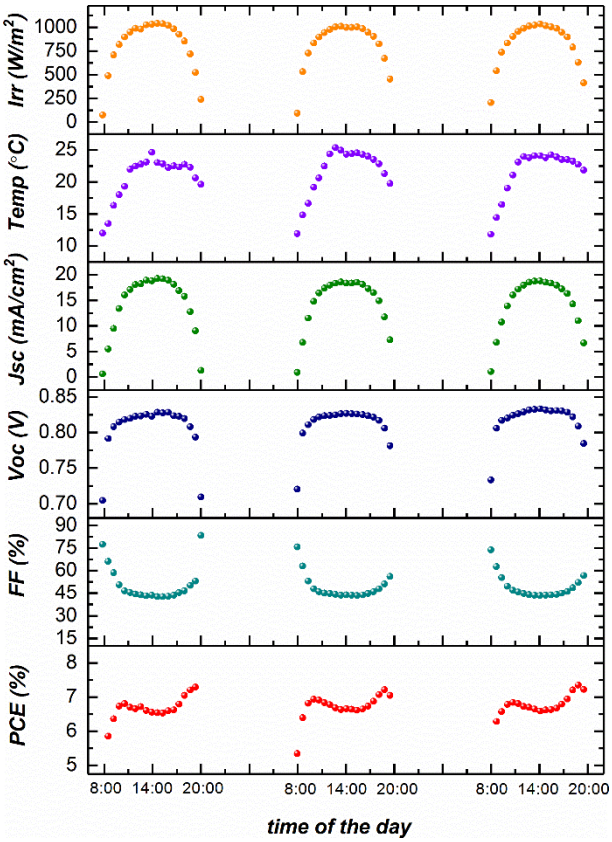

Figure 8. Stability analysis according to protocol ISOS-O2 (outdoor tests): evolution of irradiance, temperature and PV parameters during daytime over 3 consecutive days for an encapsulated solar cell monitored in Barcelona, Spain.

Keyword: Perovskite solar cells

F. De Rossi*, J. Barbé, D. M. Tanenbaum, L. Cinà, L. A. Castriotta, V. Stoichkov, Z. Wei, W. C. Tsoi, J. Kettle, A. Sadula, J. Chircop, B. Azzopardi, H. Xie, A. Di Carlo, M. Lira-Cantú, E. A. Katz, T. M. Watson, and F. Brunetti

An inter-laboratory study on the stability of all-printable HTM-free perovskite solar cells

ToC figure

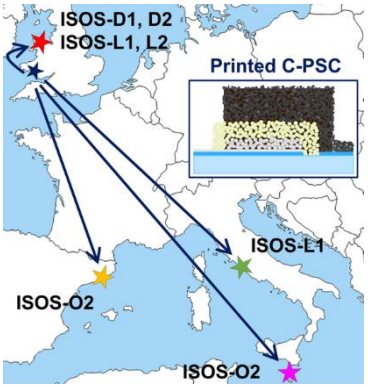

Printable Carbon-based Perovskite Solar Cells on tour. Inter-laboratory studies on perovskite solar cells stability are still limited. This work involves 5 laboratories and applies the ISOS protocols to assess the cells stability in the dark (ISOS-D), under illumination (ISOS-L) and outdoors (ISOS-O). Devices are reported to be stable in the dark for >1000 hours and outdoors for 30 days in 2 different sites, while their stability under continuous illumination depends on load and lamp spectrum.

Supporting Information

An inter-laboratory study on the stability of all-printable HTM-free perovskite solar cells

Francesca De Rossi, Jérémy Barbé, David M. Tanenbaum, Lucio Cinà, Luigi A. Castriotta, Vasil Stoichkov, Zhengfei Wei, Wing Chung Tsoi, Jeffrey Kettle, Artem Sadula, John Chircop, Brian Azzopardi, Haibing Xie, Aldo Di Carlo, Monica Lira-Cantú, Eugene A. Katz, Trystan M. Watson, and Francesca Brunetti*

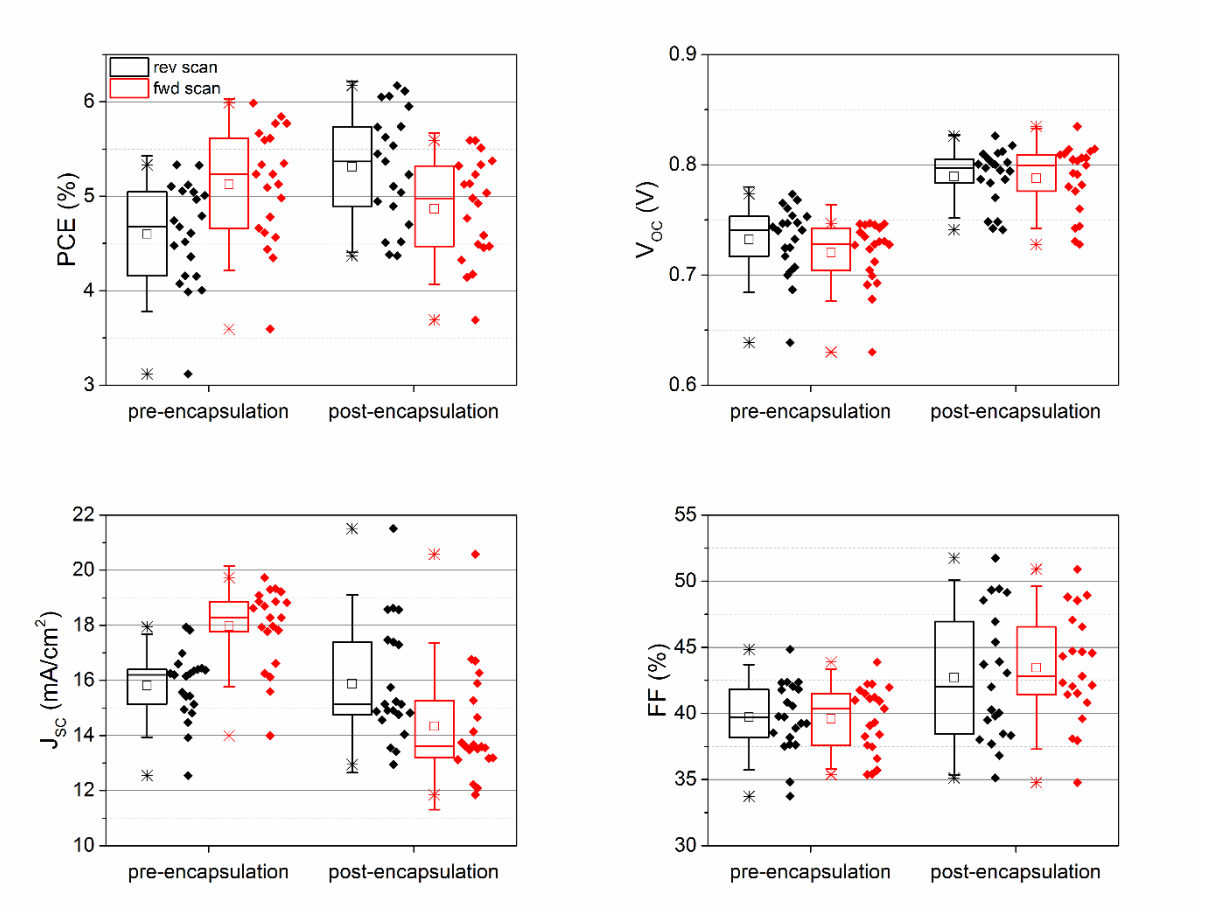

Figure S1. PV parameters distribution before and after encapsulation for 21 cells, masked to 0.5 cm^2 area. Scans were performed from 1 V to -0.1 V at 20 mVs^{-1}, in both reverse (V_{OC} to J_{SC}) and forward directions.

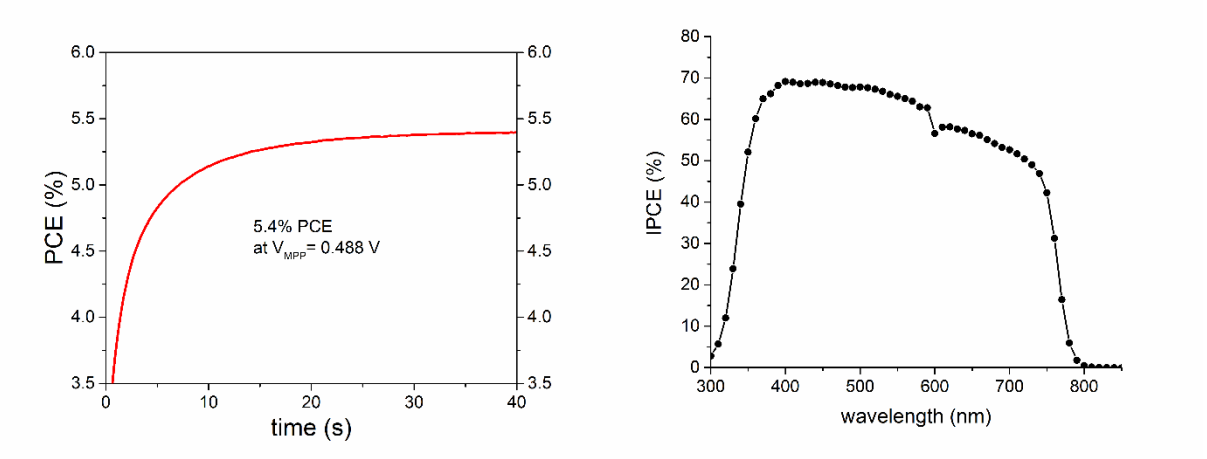

Figure S2. Stabilised PCE at maximum power point and IPCE spectrum for a typical cell, whose active area is masked to 0.5 cm^2. Spot size for IPCE measurements is 1 mm x 5 mm (0.05 cm^2). The J_{SC} value is calculated by integrating the IPCE curve is 14.9 $mA \cdot cm^{-2}$.

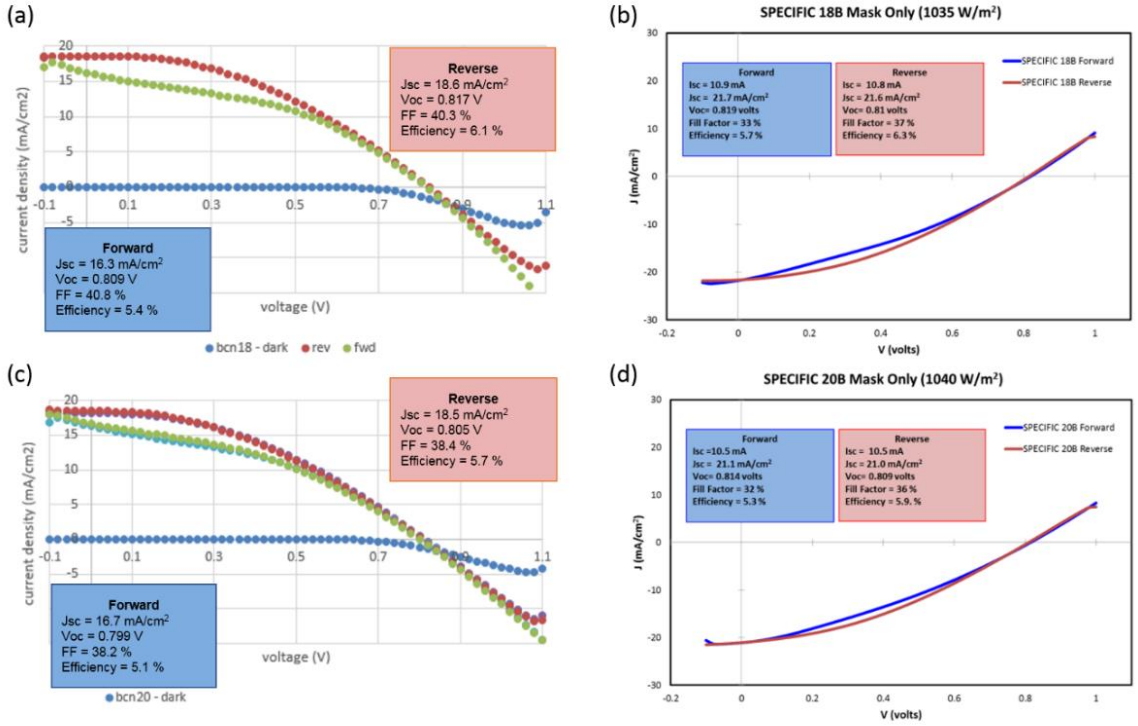

Figure S3. J-V curves for the same devices, n.18 and n.20 respectively, recorded at the manufacturing laboratory after encapsulation (a, c) and at the characterization laboratory after reception and before starting the stability tests (b, d). J-V scans in both reverse and forward directions were performed by both laboratories at the same scan rate of 20 $mV \cdot s^{-1}$. No degradation was observed.

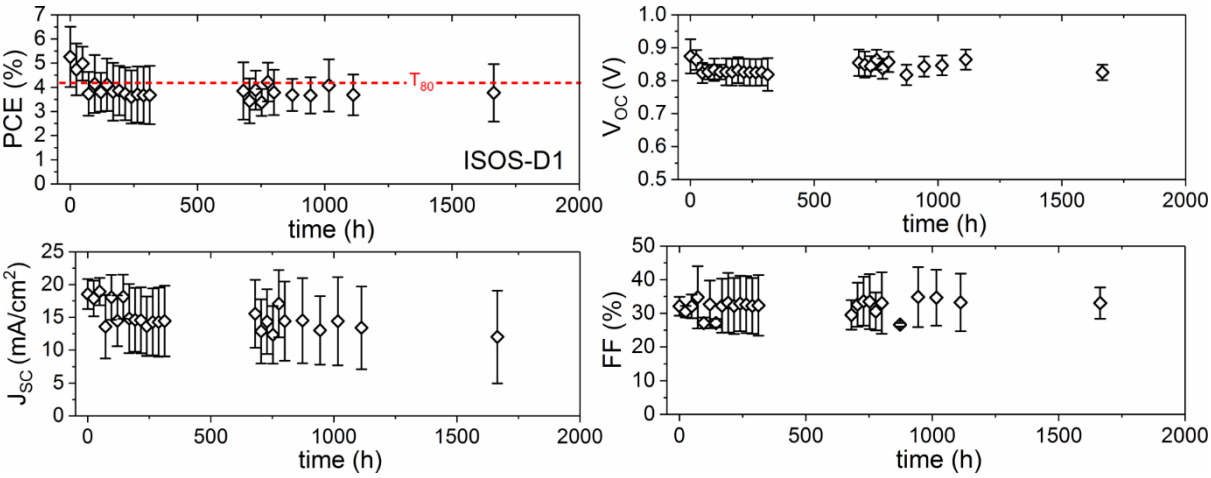

Figure S4. ISOS-D1 stability test (dark, room temperature, ambient humidity): PV parameters over time (average of 3 cells, 0.5 cm^2 masked area). The dashed line indicates T_{80} value for PCE.

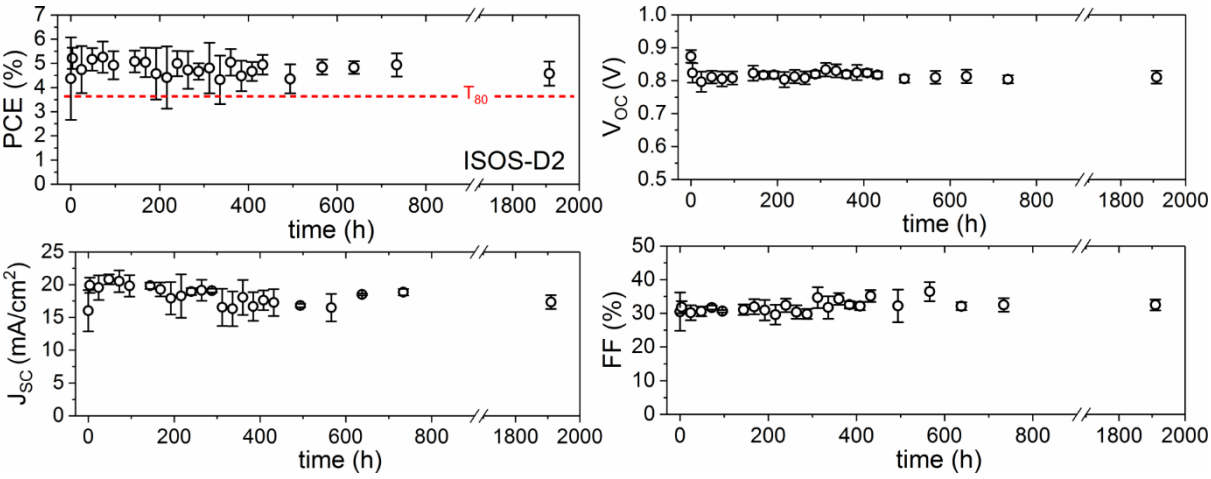

Figure S5. ISOS-D2 stability test (dark, 65 °C, ambient humidity): PV parameters over time (average of 3 cells, 0.5 cm^2 masked area). The dashed line indicates T_{80} value for PCE.

Table S1. PV parameters for encapsulated and not encapsulated cells used for Raman measurements, before and after ageing at ISOS-D1 conditions (dark, room temperature).

		V_{oc} (V)	J_{SC} (mA/cm^2)	FF (%)	PCE (%)
Encapsulated					
fresh	REV	0.787	15.1	36.8	4.4
	FOR	0.810	13.7	44.7	5.0

aged	*REV*	*0.900*	*17.2*	*34.5*	*5.4*
	FOR	*0.880*	*14.7*	*39.6*	*5.1*
Not Encapsulated					
fresh	REV	0.802	21.5	35.1	6.1
	FOR	0.782	20.6	34.8	5.6
aged	*REV*	*0.920*	*20.5*	*33.5*	*6.3*
	FOR	*0.910*	*19.6*	*31.4*	*5.6*

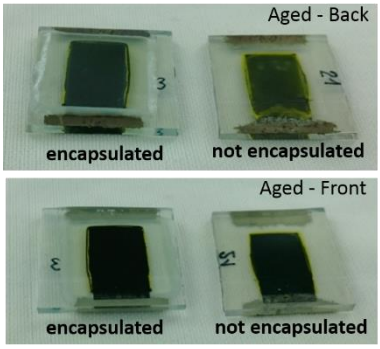

Figure S6. Pictures of the encapsulated and not encapsulated cells used for Raman measurements, after being aged at ISOS-D1 conditions (dark, room temperature) for 1000 hours: from the back side showing the carbon electrode (top photos) and from the front side, i.e. through the glass, showing the m-TiO_2 (bottom photos).

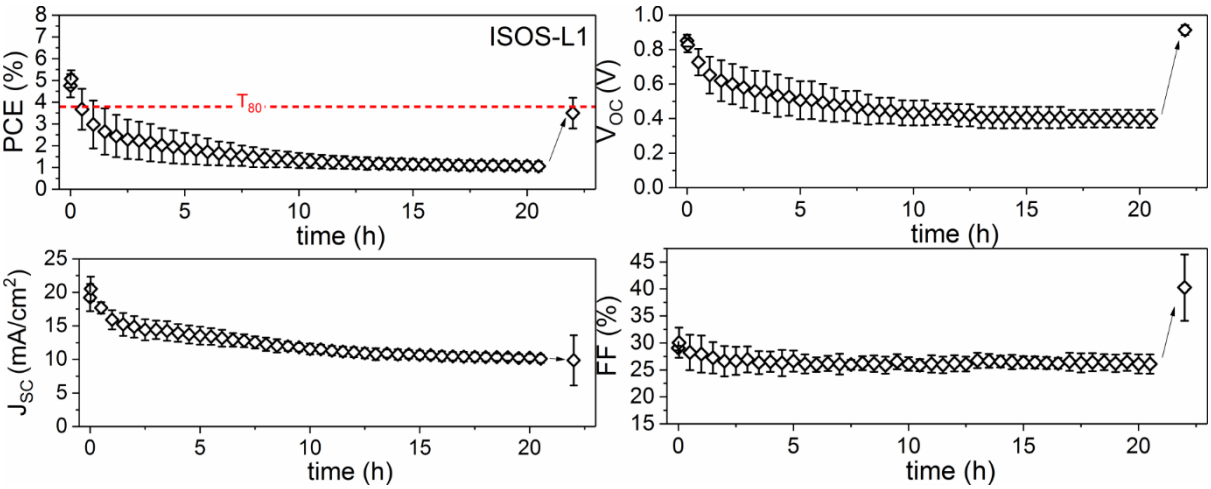

Figure S7. Light soaking tests on encapsulated cells, under ISOS-L1 conditions (1 sun, room temperature and ambient humidity). Reported data are averaged values over 3 devices with 0.5 cm^2 masked area. The cells were tested again once shipped back to the manufacturing laboratory, showing partial recovery.

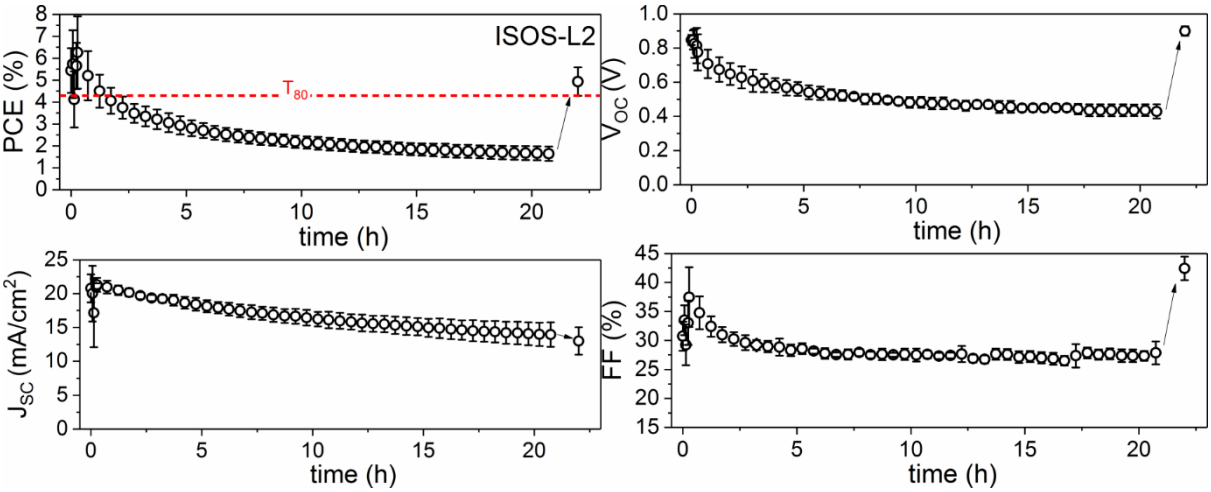

Figure S8. Light soaking tests on encapsulated cells, under ISOS-L2 (1 sun, at 65 °C and ambient humidity). Reported data are averaged values over 3 devices with 0.5 cm^2 masked area. The cells were tested again once shipped back to the manufacturing laboratory, showing partial recovery.

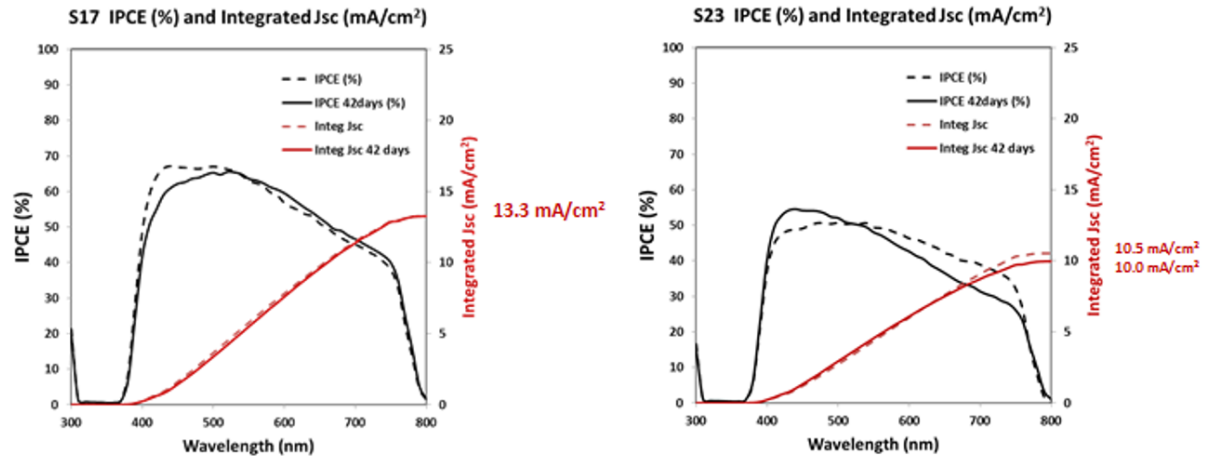

Figure S9. IPCE spectra of the 2 C-PSCs before and after the outdoor test in Barcelona: the cutoff below 380 nm is due to the UV filter applied on the cells and used throughout the ageing. The integrated J_{SC} did not change, the IPCE spectra modified their shape, denoting likely changes at the interfaces.

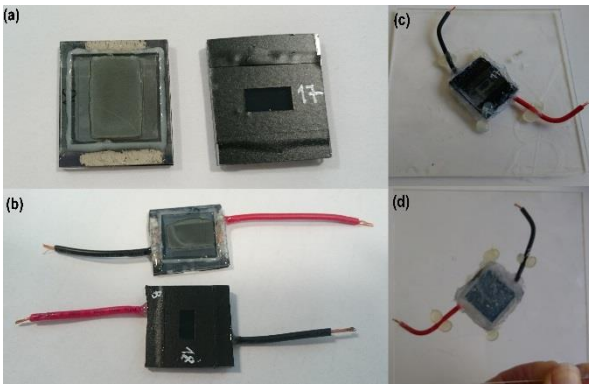

Figure S10. Photos of encapsulated cells i.e. glass cover and UV-curable resin (primary encapsulation) masked to 0.5 cm^2 with black tape for (a) indoor and (b, c, d) outdoor tests. For the latter, wires were ultrasonically soldered to the cell contacts (b), UV filter was attached on the front of the cell (c), waterproof silicon (secondary encapsulation) to cover the back and attach the cell on plexiglass tiles to ease the handling.